







V1298 Tau with TESS: Updated Ephemerides, Radii, and Period Constraints from a Second Transit of V1298 Tau e

ADINA D. FEINSTEIN ^{1,*} TREVOR J. DAVID ^{2,3} BENJAMIN T. MONTET ^{4,5} DANIEL FOREMAN-MACKEY ²
JOHN H. LIVINGSTON ⁶ AND ANDREW W. MANN ⁷

¹*Department of Astronomy and Astrophysics, University of Chicago, Chicago, IL 60637, USA*

²*Center for Computational Astrophysics, Flatiron Institute, New York, NY 10010, USA*

³*Department of Astrophysics, American Museum of Natural History, New York, NY 10024, USA*

⁴*School of Physics, University of New South Wales, Sydney, NSW 2052, Australia*

⁵*UNSW Data Science Hub, University of New South Wales, Sydney, NSW 2052, Australia*

⁶*Department of Astronomy, University of Tokyo, 7-3-1 Hongo, Bunkyo-ku, Tokyo 113-0033, Japan*

⁷*Department of Physics and Astronomy, The University of North Carolina at Chapel Hill, Chapel Hill, NC 27599, USA*

Submitted to ApJL

ABSTRACT

V1298 Tau is a young (20–30 Myr) solar-mass K star hosting four transiting exoplanets with sizes between $0.5 - 0.9R_J$. Given the system’s youth, it provides a unique opportunity to understand the evolution of planetary radii at different separations in the same stellar environment. V1298 Tau was originally observed 6 years ago during *K2* Campaign 4. Now, V1298 Tau has been re-observed during the extended mission of NASA’s Transiting Exoplanet Survey Satellite (*TESS*). Here, we present new photometric observations of V1298 Tau from the 10-minute *TESS* Full-Frame Images. We use the *TESS* data to update the ephemerides for V1298 Tau bcde as well as compare newly observed radii to those measured from the *K2* light curve, finding shallower transits for V1298 Tau bcd in the redder *TESS* bandpass at the $1 - 2\sigma$ level. We suspect the difference in radii is due to starspot-crossing events or contamination from nearby faint stars on the same pixels as V1298 Tau. Additionally, we catch a second transit of V1298 Tau e and present a new method for deriving the marginalized posterior probability of a planet’s period from two transits observed years apart. We find the highest probability period for V1298 Tau e to be in a near 2:1 mean motion resonance with V1298 Tau b which, if confirmed, could make V1298 Tau bcde a 4 planet resonant chain. V1298 Tau is the target of several ongoing and future observations. These updated ephemerides will be crucial for scheduling future transit observations and interpreting future Doppler tomographic or transmission spectroscopy signals.



Keywords: Exoplanets (498) — Pre-main sequence (1289) — Starspots (1572) — Stellar activity (1580)

1. INTRODUCTION

Planetary radii are expected to evolve over time, due to a variety of endogenous and exogenous physical pro-

cesses, such as gravitational contraction, atmospheric heating and mass-loss, and core-envelope interactions (e.g. Owen & Wu 2013; Lopez & Fortney 2013; Jin et al. 2014; Chen & Rogers 2016; Ginzburg et al. 2018). The most dramatic changes are believed to occur at early stages, when planets are still contracting and radiating away the energy from their formation, and when host stars are heating planetary atmospheres with high levels of X-ray and ultraviolet radiation. Since the size

Corresponding author: Adina D. Feinstein;

 @afeinstein20;  afeinstein20;

afeinstein@uchicago.edu

* NSF Graduate Research Fellow

evolution of any individual planet is believed to be slow relative to typical observational baselines, the best way to make inferences about the size evolution of exoplanets is by measuring the sizes of large numbers of planets across a range of ages.

NASA’s Transiting Exoplanet Survey Satellite (*TESS*; Ricker et al. 2015) has made significant inroads toward this objective. *TESS*’s observations of $\sim 90\%$ of the sky have allowed for exoplanet transit searches around stars ranging from the pre-main sequence to the giant branch. It is through targeted surveys of young stars such as the THYME (e.g. Newton et al. 2019), PATHOS (e.g. Nardiello et al. 2020), and CDIPS (e.g. Bouma et al. 2020) surveys, along with case studies of individual systems (e.g. Benatti et al. 2019; Plavchan et al. 2020; Hedges et al. 2021; Zhou et al. 2021) that the timeline for planetary radii evolution can be pieced together.

The V1298 Tau planetary system is one particularly valuable benchmark for understanding the size evolution of exoplanets. V1298 Tau is a pre-main sequence, approximately solar-mass star that was observed in 2015 by NASA’s *K2* mission (Howell et al. 2014). Analysis of the *K2* data revealed the presence of four transiting planets, all with sizes between that of Neptune and Jupiter (David et al. 2019a,b). There are no other known examples of exoplanetary systems with so many planets larger than Neptune interior to 0.5 au, despite the high completeness of the *Kepler* survey to large ($> 5 R_{\oplus}$), close-in planets. This observation raises the possibility of a causal connection between the extreme youth of V1298 Tau and the uncommonly large sizes of its planets.

The youth of V1298 Tau was initially established on the basis of its strong X-ray emission (Wichmann et al. 1996), high photospheric lithium abundance (Wichmann et al. 2000), and proper motion measurements (Frink et al. 1997). An additional recent blind search for co-moving stars using Gaia DR1 astrometry data found V1298 Tau was co-moving with 8 other stars (Group 29 in Oh et al. 2017). Luhman (2018) conducted a kinematic study of the Taurus star-forming region using Gaia DR2 and found new members of this group. With this new sample, they derived an age of ~ 40 Myr. However, more recent analyses based on Gaia EDR3 astrometry suggests V1298 Tau may belong to either the D2 or D3 subgroups of Taurus, both of which have estimated ages $\lesssim 10$ Myr (Gaidos et al. 2021; Krolkowski et al. 2021). Other studies focused specifically on the V1298 Tau system have estimated its age to be 23 ± 4 Myr from comparison with empirical and theoretical isochrones (David et al. 2019b), or 28 ± 4 Myr from

isochrone fitting to the Luhman (2018) Group 29 membership list given Gaia EDR3 data (Johnson et al. 2021). While the precise age of V1298 Tau remains uncertain, most estimates fall in the 10–40 Myr range and we adopt $t \approx 20\text{--}30$ Myr.

Given the system’s youth and potential to reveal information about the initial conditions of close-in planetary systems (e.g. Owen 2020; Poppenhaeger et al. 2021), V1298 Tau has been the target for extensive follow-up observations. These include efforts to constrain planet masses with radial velocities (Beichman et al. 2019; Suárez Mascareño et al. 2021), measure the spin-orbit alignments of planet c (Feinstein et al. 2021) and planet b (Johnson et al. 2021; Gaidos et al. 2021), measure or constrain atmospheric mass-loss rates for the innermost planets (Schlawin et al. 2021; Vissapragada et al. 2021), and an approved program to study the planetary atmospheres using the James Webb Space Telescope (JWST; Desert et al. 2021).

Here we report on newly acquired *TESS* observations of V1298 Tau which help to refine the orbital ephemerides of the transiting planets and enable comparison of the planet sizes inferred from two different telescopes with different bandpasses (*TESS* and *Kepler*). The goal of this letter is to provide a quick analysis of the new *TESS* data to help improve the transit timings for follow-up observations being performed by the community. We describe the observations and light curve extraction in Section 2. In Section 3, we present our light curve modeling and method for computing the marginalized posterior probability of a transiting planet’s period from two transits observed with a large time gap. In Section 4, we discuss the differences in measured transit parameters between *K2* and *TESS* data. We conclude in Section 5.

2. TESS OBSERVATIONS

During its Extended Mission Cycle 4, *TESS* is re-observing many of the previous *K2* fields. V1298 Tau (TIC 15756231) was observed by *TESS* in Sectors 43 (UT 16 Sep 2021 to UT 12 Oct 2021) and 44 (UT 12 Oct 2021 to UT 06 Nov 2021). For Sectors 43 and 44, we used the 2-minute light curve created by the Science Processing Operations Center pipeline (SPOC; Jenkins et al. 2016) and binned the data down to 10-minute cadence.

We compared these new light curves to our original FFI light curves. We created our initial light curves from the *tica*-processed FFIs by modeling the point-spread function (PSF) of V1298 Tau and the two nearby bright sources (white x’s in Figure 1), following the PSF

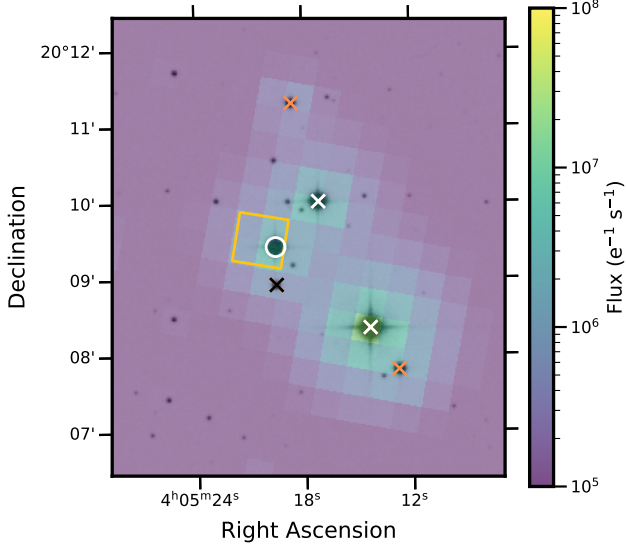


Figure 1. The *TESS* tica FFI target pixel file (TPF) overlaid with a sky image of V1298 Tau taken with the Digitized Sky Survey (DSS) r-band. V1298 Tau is highlighted by the white circle; nearby sources with *TESS* magnitudes < 14 are marked with x's. The two stars with white x's (TICs 15756226 and 15756240) were simultaneously fit during our PSF-modeling. The one star with black x (TIC 15756236) is a bright nearby source that was not included in our PSF-modeling. While aperture photometry would be feasible for this system (yellow square), we found fitting three point-spread functions to the brightest stars extracted the cleanest light curve for V1298 Tau. ☉

modeling routine in Feinstein et al. (2019).¹ In summary, we calculated and maximized the likelihood value of seven parameters per each Gaussian: the x and y width, 2D position, amplitude, a rotational term, and a background term. The Gaussian fits are allowed to vary at each time step. Aperture photometry (example square aperture shown in Figure 1) provided a light curve with more systematics and scatter. We found that modeling the three brightest stars simultaneously, including V1298 Tau, with a 2D Gaussian created the least contaminated light curve. Our extracted light curve is shown in the top row of Figure 2.

3. ANALYSIS

We simultaneously modeled the transits of V1298 Tau bcd and the stellar variability using the open-source packages *exoplanet* (Foreman-Mackey et al. 2021a,b) and *PyMC3* (Salvatier et al. 2016). Transit timings were originally identified using updated ephemerides from *Spitzer* (Livingston et al. in prep)

and we account for potential transit timing variations (TTVs) in our model using *exoplanet*'s *TTVOrbit* function. This functionality allows us to fit the individual transit time per each transit, while all other orbital and planetary parameters remain the same.

exoplanet.TTVOrbit worked well when fitting V1298 Tau bcd, due to there being multiple transits. However, with V1298 Tau e being a single-transit event, we found the GP model with TTVs optimized our hyperparameters to accommodate for transits where there were none; as such, we used a model without accounting for TTVs to fit the parameters for V1298 Tau e. All other transit parameters (presented in Table 1) were initialized using values from David et al. (2019a). We assumed a quadratic limb darkening law, following the reparameterization described by Kipping (2013); this method allows for an efficient and uniform sampling of limb-darkened transit models.

Since the tica FFIs do not provide an error estimate, we fit for flux errors within our Gaussian Process (GP) model. We define the flux error as

$$\sigma_y = e^{\ln(\sigma_l)} + y^2 e^{2\ln(\sigma_j)} \quad (1)$$

where y is the normalized flux array about zero, and σ_l and σ_j are used to define the light curve noise and in-transit jitter, which is designed to capture the added noise produced by starspot crossing events. σ_l and σ_j are also used as the first and second terms in our rotation model, which we defined as a stochastically-driven, damped harmonic oscillator, defined by the *SHOTerm* in *celerite2* (Foreman-Mackey et al. 2017).

We modeled the background within our GP. We defined a quadratic trend with respect to time for varying the background flux, where each polynomial coefficient was drawn from a normal distribution. Then, we generated a Vandermonde matrix (A) of time. This is a way of introducing a polynomial least-squares regression with respect to time. The final background flux was calculated by taking $bkg = A \cdot trend$.

We performed an MCMC sampling fit to each parameter.² We ran 3 chains with 500 tuning steps and 5000 draws. We discarded the tuning samples from the posterior chains before calculating our best-fit parameters. Our results are presented in Table 1, along with our selected priors for each parameter we fit. These results are consistent with our original tica-processed point-spread function modeled light curves. We verified our chains converged via visual inspection and following the diagnostic provided by Geweke (1992).

¹ Our PSF-modeled light curves are available [here](#).

² A Jupyter notebook detailing our model can be found [here](#).

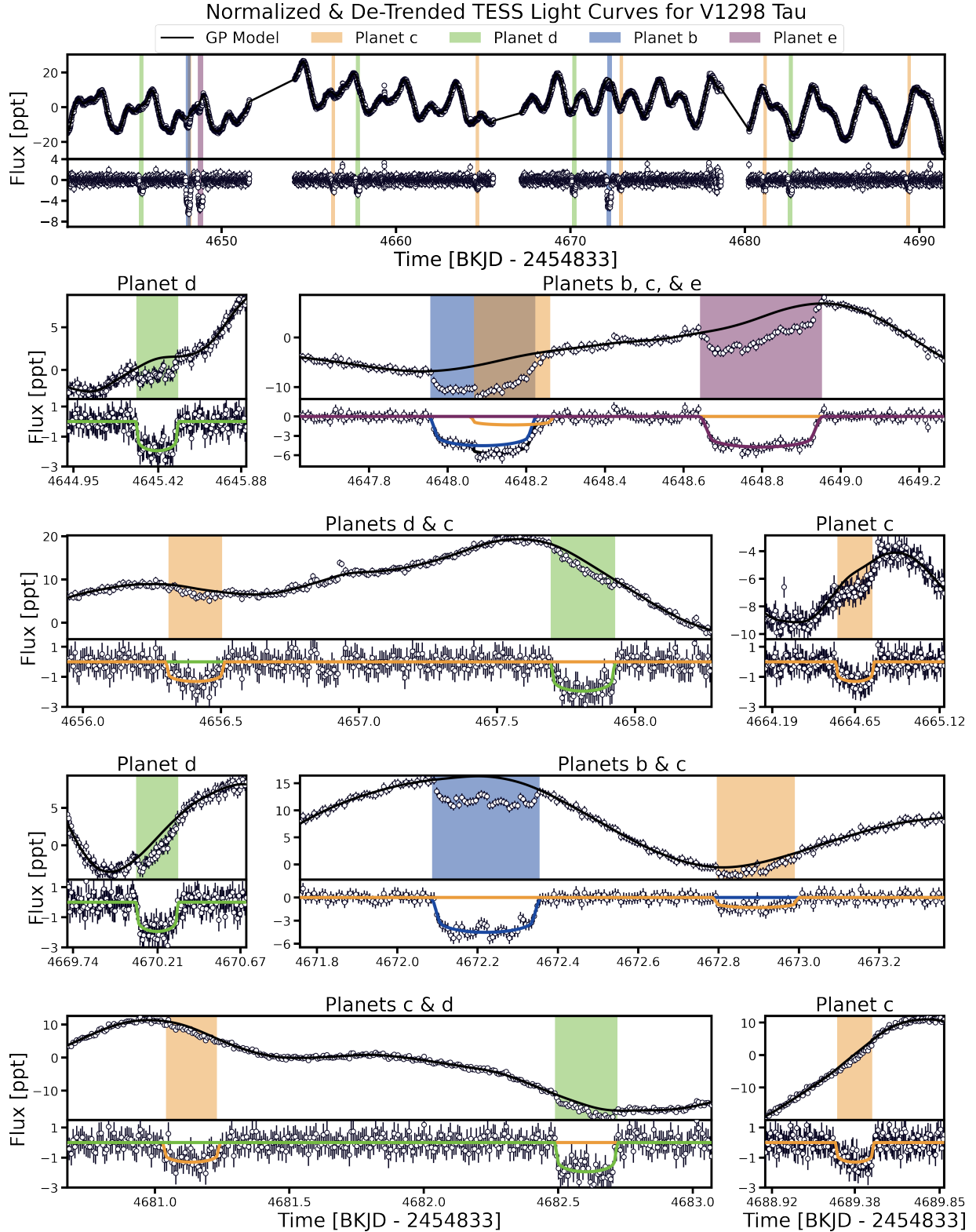


Figure 2. V1298 Tau extracted light curve from the SPOC-processed light curve for Sectors 43 and 44, with transits of V1298 Tau bcde highlighted by color. Each subplot contains the raw, normalized *TESS* flux (top) and the GP model removed flux (de-trended flux; bottom). Top row: extracted light curve with over plotted with our best-fit GP model for stellar variability (black). Bottom three rows: zoomed-in regions around the transits present in the *TESS* data. The GP best-fit model is over-plotted on the raw, normalized flux. The best-fit transit models are over-plotted on the de-trended flux. For overlapping transits (sub-panel “Planets b, c, & e”), the sum of the transits is blotted in black. ☉

We present our final GP model for stellar variability, planet transits, and best-fit transit models in Figure 2. There is a $\sim 1\%$ flare at *TESS* BKJD ≈ 4659.18 that we do not fit.

3.1. Constraining V1298 Tau e’s Period

V1298 Tau (EPIC 210818897) was observed during Campaign 4 of the *K2* mission. There was a single transit of V1298 Tau e in the original *K2* data, which occurred roughly in the middle of the campaign. Since no other transits were detected, this provides a lower period limit of 36 days. Additionally, there was only 1 transit of V1298 Tau e between the two *TESS* sectors, which provides a new lower limit of 42.7 days. Using the original transit timing from *K2* and this new transit timing from *TESS*, we developed a new method for constraining the period of V1298 Tau e. For this analysis, we used the EVEREST 2.0 (Luger et al. 2018) version of the *K2* light curve.

Determining the period of a planet from two transits with a significant time gap between surveys has previously been constrained by fitting for orbital periods using MCMC sampling, phase-folding all available transits on the derived transit times and periods, and computing a reduced- χ^2 fit to a flat line (Becker et al. 2019). Orbital periods providing a match to a flat line with a likelihood exceeding some threshold are then ruled out. In our new method, we fit transit models of many discrete periods at each step of the MCMC sampler, rather than post-processing from our posterior.

First, we de-trended a localized 1-day region around the transit midpoint of V1298 Tau e in the *K2* and *TESS* light curves, assuming a constant transit depth and allowing the other transit parameters, θ to vary. Then, we fit a discrete period model, allowing all other transit parameters to vary. We set the GP model to sample over discrete periods ranging from 38 – 56 days. We fit for θ assuming a constant transit depth between the *K2* and *TESS* observations. We assumed there is no correlation between the other transit parameters and the period we are fitting for. For each step in our MCMC fit, we compute all possible periods

$$P = \frac{1}{q} (T_{mid,TESS} - T_{mid,K2}) \quad (2)$$

where T_{mid} are the transit midpoints from *K2* and *TESS* and q is an integer representing a specific harmonic. We assume a uniform prior, i.e. we have no prior preference for a specific harmonic. At each step of the sampling process, we compute a new light curve with different orbital periods, given by Equation 2. The log

likelihood of the new light curves models are calculated as

$$\log \mathcal{L}_q = [\log p(X|\theta^k, q^k = n)]_n \quad (3)$$

where X is the *TESS* light curve and n is the period being tested. We additionally calculate the sum of all log likelihoods for each period

$$\log \mathcal{L} = \log \sum_q p(q) p(X|\theta^k, q) \quad (4)$$

The summation of all log likelihoods is used to compute the posterior likelihood for each sampled value of q . This analysis assumes a circular orbit for planet e and uses stellar density constraints via priors on the stellar mass and radius.³

We ran 3 chains with 500 tuning steps and 5000 draws. We discarded the tuning steps before our analysis. Our results are presented in Figure 3, where we plot the median period for each tested harmonic against the posterior probability of each harmonic.

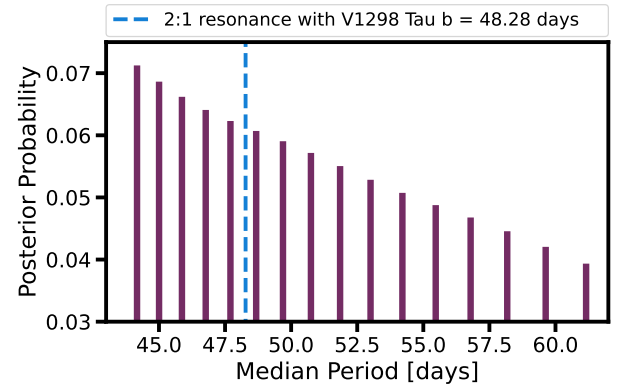


Figure 3. Our calculated posterior probability to constrain the period of V1298 Tau e using transit timings from *K2* and *TESS*. We tested discrete periods from $q = 38 - 56$ days and find the most likely period to be 44.17 days. The 2:1 resonance (48.28 days) with V1298 Tau b is plotted as the dashed vertical line. ☞

We find the most likely period of V1298 Tau e to be 44.17 days. We provide all tested periods and posterior probabilities in Table 2. Our period estimate is at a 4- σ disagreement with the period measured in a potential radial velocity signal for V1298 Tau e presented in Suárez Mascareño et al. (2021). This derived period estimate suggests that V1298 Tau e is in a near 2:1 mean motion resonance with V1298 Tau b. If the period of

³ A Jupyter notebook detailing our model for constraining the period for V1298 Tau e can be found [here](#).

V1298 Tau e is confirmed to be within the presented range, this could indicate that V1298 Tau bcde are in a nearly 4-planet resonant chain.

Independent ground-based monitoring of the system may be able to observe another transit of the outermost known planet in this system. Using the Transit Service Query Form on the NASA Exoplanet Archive (Akeson et al. 2013), we provide several potential transit mid-point events for all fitted periods in Table 2.

4. DIFFERENCES IN MEASURED RADII

We compare the differences in transit R_p/R_* between the *K2* and *TESS* data in Figure 4. We masked regions in the light curve where transits overlapped. The residuals of the *TESS* light curve with our model (color) are plotted as well. For V1298 Tau bcd, the transit radii are smaller in the *TESS* data, while only the measured radius for V1298 Tau e is larger (Figure 4, bottom panel).

The error bars from our MCMC fit on the radii of the planets are smaller than that provided by David et al. (2019b). We initialized our MCMC to fit the transit depths with a Gaussian distribution around the fitted values from David et al. (2019b) with a standard deviation of 0.1 (Table 1). The smaller errors could be due to the higher cadence of the *TESS* data (10-minutes vs. 30-minutes) or due to larger spot-crossing events in *K2*. Larger spot-crossings would result in a greater uncertainty of the transit depth, and this is potentially evident in comparing the transit depth and shape for V1298 Tau e (Figure 4).

4.1. Radii of V1298 Tau bcd

A shallower transit depth at redder wavelengths is supported by the dusty outflow model presented in Wang & Dai (2019), while transits in the optical probe lower atmospheric pressures, resulting in larger transit depths (Gao & Zhang 2020). Therefore, the difference in transit depths could be due to the difference in bandpass wavelength coverage between *Kepler* (400-900 nm; Howell et al. 2014) and *TESS* (600-1000 nm; Ricker et al. 2015).

The ability of a planet to retain hazes/transition hazes is negatively correlated with its equilibrium temperature, T_{eq} , internal temperature T_{int} , and positively correlated with mass, M_{core} . V1298 Tau bcde have calculated $T_{eq} < 1000$ K, assuming an albedo = 0 (David et al. 2019a). Young planets are believed to have high T_{int} due to ongoing gravitational contraction (Gu et al. 2004). The combination of these two parameters make these planets more likely to host extended high-altitude hazes in their atmospheres, while outflow winds lead to the formation of transition hazes (Gao & Zhang 2020).

However, it is more likely we are seeing either contamination/dilution from another nearby star or the presence of starspots. As highlighted by a black x in Figure 1, there is a bright (*TESS* magnitude < 14) just next to V1298 Tau. Since we did not include this source in our light curve PSF-modeling, it is possible there is some light from this source in our data, therefore making the transits of V1298 Tau bcd appear $\sim 10\%$ shallower in our *TESS* data than the original *K2* measurements. The *TESS* Input Catalog (Stassun et al. 2018) lists a contamination value of 0.315 for V1298 Tau, which could sufficiently produce the decrease in transit depths presented here.

We check for signs of dilution by creating light curves for individual pixels around V1298 Tau and measure the transit depths of V1298 Tau b and V1298 Tau e (Figure 4). We localized a 1-day window around each transit and computed the a χ^2 -fit using a transit model computed with *batman* (Kreidberg 2015) and an underlying 2nd order polynomial. We find the transit depths to decrease falling off of the pixels centered on V1298 Tau. While fitting the *TESS* PSF with a 2D Gaussian function is a reasonable approximation, it is not the perfect model. It is possible that this light curve is diluted from nearby stars, including TIC 15756226, which is the closest (separation = 49.15") star with $T_{mag} = 13.09$.

A change in transit depth could additionally be due to starspots, either from a nearby source or from the surface of V1298 Tau. In the context of starspots on V1298 Tau, both starspot/active region crossing events, where the planets directly transit over these inhomogeneities, or asymmetric starspots/active region distributions located off the transit chord could lead to differences in transit depths and shapes. In the case of starspot crossing events, we would expect to see added variability to the transit shape. Assuming we are not underestimating our error bars, this is readily seen in the transit of V1298 Tau b, both in the *TESS* and *K2* data (Figure 4).

4.2. Radius of V1298 Tau e

Contrary to V1298 Tau bcd, we measure a transit radius that is $\sim 3\sigma$ larger in the new *TESS* data than what was found in the original *K2* data (David et al. 2019a). The difference in radii could be consistent with a large scale height, low mean-molecular weight atmosphere around V1298 Tau e (de Mooij et al. 2012). It is also possible the atmosphere of V1298 Tau e is dominated by species with stronger absorption features at longer wavelengths, such as CO, H₂O, and CH₄ (Carter et al. 2009).

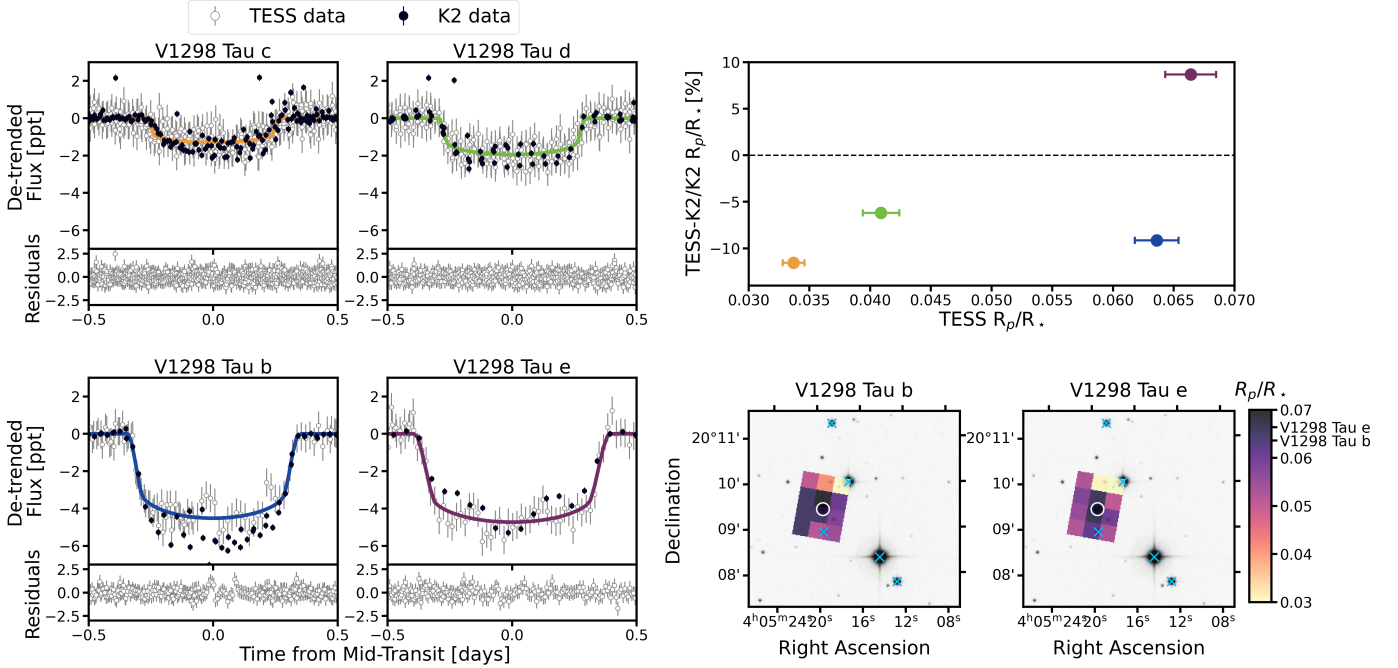


Figure 4. Left: Phase-folded *TESS* data (gray) with the new best-fit model (color) compared to the original *K2* data (black). The residuals between the *TESS* data and each fit are shown underneath. Top right: The percent difference in measured R_p/R_* from *K2* vs. *TESS* R_p/R_* . A dashed line is shown at 0% to help visually differentiate between measured increases and decreases in planetary radii. The transit depths for V1298 Tau bcd are shallower in the new *TESS* data, while the transit depth for V1298 Tau e is deeper. Bottom right: The change in R_p/R_* as a function of pixel for V1298 Tau b (left) and V1298 Tau e (right) overlaid with a sky image of V1298 Tau taken with the Digitized Sky Survey (DSS) r-band. We speculate the variation in transit depths could be due to contamination from nearby bright stars or starspot crossing events. ☞

We find it is more likely that the original single transit of V1298 Tau e was filled-in via spot-crossing events, making it appear shallower in the *K2* observations. Young stars are known to have very high spot coverage, anywhere from 30-80% (Grankin 1999; Gully-Santiago et al. 2017; Feinstein et al. 2020). It is therefore likely the surface of V1298 Tau is dominated by stellar inhomogeneities. This hypothesis is further strengthened by comparing the transit shape between the two data sets (Figure 4). The center of the *K2* transit is deeper than the edges and is consistent with the most recently observed transit depth. The lower contrast in starspot signals at longer wavelengths could potentially explain why the transit depth is consistent deeper in the *TESS* observations. Additionally, there is noise in-transit in the *TESS* data that could potentially be more starspot crossing events.

Future *TESS* 20-second and 2-minute data may have the temporal resolution needed to yield insight into if there is evidence of starspot crossing events. Our transit of V1298 Tau e from the FFIs shows some structure. At the 10-minute cadence, it is hard to rule out noise as the source of this structure. However if there is such evidence of starspot crossings in the higher-cadence *TESS*

observations, it would be interesting if any of the events dilutes the transit enough to result in a similar transit depth to that which was seen in *K2*.

5. CONCLUSIONS

We present updated ephemerides for all four known planets in the V1298 Tau system. Our GP model accounts for TTVs for V1298 Tau bcd. The transit timings for V1298 Tau c deviates from a linear ephemeris by -30 to 30 minutes, and V1298 Tau d deviates by -5 to 5 minutes. Additionally, we note the transits of V1298 Tau bcd occur 1.92 later, and 5.83 and 4.72 hours earlier than what is expected if we extrapolate forward the ephemerides from David et al. (2019b).

We detected a second transit of V1298 Tau e; this new transit time in combination from the transit observed with *K2* allowed us to place tighter constraints on the period of the outermost planet. Our revised radius for planet e makes it now the largest planet in the system and extends an intriguing size-separation correlation in V1298 Tau such that planet size increases monotonically with separation.

We find the transit depths of V1298 Tau bcd as observed by *TESS* are shallower than those observed by

K2 by $1 - 2\sigma$, with the exception of V1298 Tau e, which is $\sim 3\sigma$ larger. While this could possibly be due to ongoing dusty outflows that make the transit depth appear shallower, it is more likely the differences are due to starspot crossing events, asymmetric starspots off the transit chord, or contamination from nearby faint stars in the same *TESS* pixels are V1298 Tau. Modeling potential starspot crossing events could be accomplished using the 2-minute and 20-second cadence light curves, which will be available in the coming months.

The youth of these planets could additionally favor hosting haze-dominated atmospheres. However, without mass estimates for V1298 Tau bcde, it is difficult to determine if this is the cause of the different transit depths measured between the *K2* data and our presented work. Radial velocity mass measurements are challenging for young planets due to underlying stellar activity.

Through an intensive radial velocity campaign, Suárez Mascareño et al. (2021) presented a new mass detection for V1298 Tau b and V1298 Tau e. Our updated radius estimate for V1298 Tau b in combination with the mass estimate provided by Suárez Mascareño et al. (2021) would yield a density of 1.29 g/cm^3 , which is slightly higher than what was originally reported. Our updated radius for V1298 Tau e would yield a lower density of 2.04 g/cm^3 , which is still within a $1\text{-}\sigma$ agreement with Suárez Mascareño et al. (2021). However, the period estimate for V1298 Tau e is at a $4\text{-}\sigma$ disagreement for the period estimate provided in this study and at a $2\text{-}\sigma$ disagreement with the minimum period constraint provided by this new *TESS* data.

A more promising approach to measuring the masses would be through TTVs (Agol & Fabrycky 2018). A full analysis of system parameters and TTVs from both the *K2* and *TESS* light curves, and additional *Spitzer* transit photometry will be presented in Livingston et al. (in prep). Additional transits at longer wavelengths

or simultaneous multi-band photometry or spectroscopy could corroborate the potential of constraining the properties of these young atmospheres.

We thank Rodrigo Luger for developing *showyourwork!* (Luger et al. 2021) and helping us debug this letter. We thank Chas Beichman, Sarah Blunt, Jacob Bean, and Darryl Seligman for helpful comments on our *TESS* proposal (DDT 036) and thoughtful conversations. We thank our anonymous referee for their thoughtful insights which improved the quality of this manuscript. ADF acknowledges support from the National Science Foundation Graduate Research Fellowship Program under Grant No. (DGE-1746045).

This research has made use of NASA’s Astrophysics Data System Bibliographic Services. This research made use of *Lightkurve*, a Python package for *Kepler* and *TESS* data analysis (Lightkurve Collaboration et al. 2018).

Facilities: *TESS* (Ricker et al. 2015), *Kepler* (Howell et al. 2014)

Software: *exoplanet* (Foreman-Mackey et al. 2021b), *EVEREST 2.0* (Luger et al. 2018), *lightkurve* (Lightkurve Collaboration et al. 2018), *matplotlib* (Hunter 2007), *PyMC3* (Salvatier et al. 2016), *starry* (Luger et al. 2019), *theano* (The Theano Development Team et al. 2016), *tica* (Fausnaugh et al. 2020), *showyourwork!* (Luger et al. 2021), *astropy* (Astropy Collaboration et al. 2013; Price-Whelan et al. 2018), *astroquery* (Ginsburg et al. 2019), *numpy* (Van Der Walt et al. 2011), *celerite2* (Foreman-Mackey et al. 2017), *batman* (Kreidberg 2015)

REFERENCES

- Agol, E., & Fabrycky, D. C. 2018, Transit-Timing and Duration Variations for the Discovery and Characterization of Exoplanets, ed. H. J. Deeg & J. A. Belmonte, 7, doi: [10.1007/978-3-319-55333-7_7](https://doi.org/10.1007/978-3-319-55333-7_7)
- Akeson, R. L., Chen, X., Ciardi, D., et al. 2013, *PASP*, 125, 989, doi: [10.1086/672273](https://doi.org/10.1086/672273)
- Astropy Collaboration, Robitaille, T. P., Tollerud, E. J., et al. 2013, *A&A*, 558, A33, doi: [10.1051/0004-6361/201322068](https://doi.org/10.1051/0004-6361/201322068)
- Becker, J. C., Vanderburg, A., Rodriguez, J. E., et al. 2019, *AJ*, 157, 19, doi: [10.3847/1538-3881/aaf0a2](https://doi.org/10.3847/1538-3881/aaf0a2)
- Beichman, C., Hirano, T., David, T. J., et al. 2019, Research Notes of the American Astronomical Society, 3, 89, doi: [10.3847/2515-5172/ab2c9d](https://doi.org/10.3847/2515-5172/ab2c9d)
- Benatti, S., Nardiello, D., Malavolta, L., et al. 2019, *A&A*, 630, A81, doi: [10.1051/0004-6361/201935598](https://doi.org/10.1051/0004-6361/201935598)
- Bouma, L. G., Hartman, J. D., Brahm, R., et al. 2020, *AJ*, 160, 239, doi: [10.3847/1538-3881/abb9ab](https://doi.org/10.3847/1538-3881/abb9ab)
- Carter, J. A., Winn, J. N., Gilliland, R., & Holman, M. J. 2009, *ApJ*, 696, 241, doi: [10.1088/0004-637X/696/1/241](https://doi.org/10.1088/0004-637X/696/1/241)
- Chen, H., & Rogers, L. A. 2016, *ApJ*, 831, 180, doi: [10.3847/0004-637X/831/2/180](https://doi.org/10.3847/0004-637X/831/2/180)

Table 1. V1298 Tau light curve fitting results and predicted ground-based transit midpoint events for V1298 Tau e.

<i>Star</i>	<i>Value</i>	<i>Prior</i>		
$R_{\star}[R_{\odot}]$	$1.33^{+0.04}_{-0.03}$	$\mathcal{G}(1.305, 0.07)$		
$M_{\star}[M_{\odot}]$	$1.095^{+0.049}_{-0.047}$	$\mathcal{G}(1.10, 0.05)$		
u_1	$0.32^{+0.20}_{-0.19}$	$\mathcal{U}[0, 1]$ in q_1		
u_2	$0.16^{+0.31}_{-0.29}$	$\mathcal{U}[0, 1]$ in q_2		
P_{rot} [days]	$2.97^{+0.03}_{-0.04}$	$\mathcal{G}(\ln 2.87, 2)$		
$\ln(Q_0)$	$0.72^{+0.24}_{-0.21}$	$\mathcal{H}(\sigma = 2)$		
ΔQ_0	4.09 ± 1.01	$\mathcal{G}(0, 2)$		
f [ppt]	$0.85^{+0.11}_{-0.19}$	$\mathcal{U}[0.1, 1]$		
<i>Light Curve</i>	<i>Value</i>	<i>Prior</i>		
μ	$-1.66^{+9.42}_{-9.28}$	$\mathcal{G}(0, 10)$		
$\ln(\sigma_l)$	$-2.499^{+4.444}_{-4.463}$	$\mathcal{G}(\ln(0.1\sigma_{\text{flux}}), 10)$		
$\ln(\sigma_j)$	$-1.36^{+4.96}_{-5.06}$	$\mathcal{G}(\ln(0.1\sigma_{\text{flux}}), 10)$		
<i>Planets</i>	<i>c</i>	<i>d</i>	<i>b</i>	<i>e</i>
T_0 [BKJD - 2454833]	$4648.16636^{+0.00269}_{-0.00339}$	$4645.41494^{+0.00172}_{-0.00157}$	$4648.09023^{+0.00129}_{-0.00132}$	$4648.79668^{+0.00121}_{-0.00114}$
P [days]	$8.2438^{+0.0024}_{-0.0020}$	$12.3960^{+0.0019}_{-0.0020}$	$24.1315^{+0.0033}_{-0.0034}$	44.1699
R_p/R_{\star}	0.0337 ± 0.0009	$0.0409^{+0.0014}_{-0.0015}$	0.0636 ± 0.0018	$0.0664^{+0.0025}_{-0.0021}$
Impact parameter, b	$0.14^{+0.14}_{-0.10}$	$0.19^{+0.12}_{-0.13}$	$0.45^{+0.05}_{-0.04}$	$0.48^{+0.06}_{-0.07}$
T_{14} [hours]	$4.66^{+0.49}_{-0.43}$	$5.59^{+0.57}_{-0.53}$	$6.42^{+0.66}_{-0.61}$	$7.44^{+0.79}_{-0.71}$
$R_p[R_{\oplus}]$	5.05 ± 0.14	6.13 ± 0.28	9.53 ± 0.32	9.94 ± 0.39
$R_p[R_J]$	0.45 ± 0.01	0.55 ± 0.03	0.85 ± 0.03	0.89 ± 0.04
TTVs [minutes]	-0.41 ± 25.38	-0.12 ± 4.08	—	—
<i>Priors</i>	<i>c</i>	<i>d</i>	<i>b</i>	<i>e</i>
T_0 [BKJD - 2454833]	$\mathcal{G}(4648.53, 0.1)$	$\mathcal{G}(4645.4, 0.1)$	$\mathcal{G}(4648.1, 0.1)$	$\mathcal{G}(4648.8, 0.1)$
$\log(P$ [days])	$\mathcal{G}(\ln 8.25, 1)$	$\mathcal{G}(\ln 12.40, 1)$	$\mathcal{G}(\ln 24.14, 1)$	$\mathcal{G}(\ln 36.70, 1)$
$\log(\text{depth}$ [ppt])	$\mathcal{G}(\ln 1.45, 0.1)$	$\mathcal{G}(\ln 1.90, 0.1)$	$\mathcal{G}(\ln 4.90, 0.1)$	$\mathcal{G}(\ln 3.73, 0.1)$
Impact parameter, b	$\mathcal{U}[0, 1]$	$\mathcal{U}[0, 1]$	$\mathcal{U}[0, 1]$	$\mathcal{U}[0, 1]$
T_{14} [days]	$\mathcal{G}(\ln 0.19, 1)$	$\mathcal{G}(\ln 0.23, 1)$	$\mathcal{G}(\ln 0.27, 1)$	$\mathcal{G}(\ln 0.31, 1)$
TTVs [days]	$\mathcal{G}(T_{0,c}, 0.1)$	$\mathcal{G}(T_{0,d}, 0.1)$	$\mathcal{G}(T_{0,b}, 0.1)$	—

NOTE— u_1 and u_2 are the limb-darkening parameters sampled following the reparameterization described by [Kipping \(2013\)](#); P_{rot} is the rotation period of V1298 Tau; $\ln(Q_0)$ is the quality factor for the secondary oscillation used to fit the stellar variability; ΔQ_0 is the difference between the quality factors of the first and second modes; f is the fractional amplitude of the second mode compared the first; μ is the mean of the light curve; σ_l and σ_j are the light curve noise and in-transit jitter. Priors are noted for parameters that were directly sampled. The distributions are as follows – \mathcal{G} : Gaussian; \mathcal{H} : Half-normal; \mathcal{U} : Uniform. σ_{flux} is the standard deviation of the light curve.

David, T. J., Petigura, E. A., Luger, R., et al. 2019a, *ApJL*, 885, L12, doi: [10.3847/2041-8213/ab4c99](#)

David, T. J., Cody, A. M., Hedges, C. L., et al. 2019b, *AJ*, 158, 79, doi: [10.3847/1538-3881/ab290f](#)

de Mooij, E. J. W., Brogi, M., de Kok, R. J., et al. 2012, *A&A*, 538, A46, doi: [10.1051/0004-6361/201117205](#)

Desert, J.-M., Adhiambo, V., Barat, S., et al. 2021, The nature, origin, and fate of two planets of a newborn system through the lens of their relative atmospheric properties, JWST Proposal. Cycle 1

Fausnaugh, M. M., Burke, C. J., Ricker, G. R., & Vanderspek, R. 2020, *Research Notes of the American Astronomical Society*, 4, 251, doi: [10.3847/2515-5172/abd63a](#)

Feinstein, A. D., Montet, B. T., Ansdell, M., et al. 2020, *AJ*, 160, 219, doi: [10.3847/1538-3881/abac0a](#)

Feinstein, A. D., Montet, B. T., Johnson, M. C., et al. 2021, arXiv e-prints, arXiv:2107.01213. <https://arxiv.org/abs/2107.01213>

Feinstein, A. D., Montet, B. T., Foreman-Mackey, D., et al. 2019, *PASP*, 131, 094502, doi: [10.1088/1538-3873/ab291c](#)

Foreman-Mackey, D., Agol, E., Ambikasaran, S., & Angus, R. 2017, *AJ*, 154, 220, doi: [10.3847/1538-3881/aa9332](#)

Table 2. Predicted transit midpoint events for V1298 Tau e.

P [days]	Posterior Prob.	Observable Dates UT		
44.1699 \pm 0.0001	0.071	21/12/2021 15:17	03/02/2022 19:22	19/03/2022 23:27
45.0033 \pm 0.0001	0.069	23/12/2021 07:17	06/02/2022 07:22	23/03/2022 07:27
45.8687 \pm 0.0001	0.066	25/12/2021 00:50	08/02/2022 21:41	26/03/2022 18:32
46.7681 \pm 0.0001	0.064	26/12/2021 20:00	11/02/2022 14:26	30/03/2022 08:52
47.7035 \pm 0.0001	0.062	28/12/2021 16:54	14/02/2022 09:47	03/04/2022 02:40
48.6770 \pm 0.0001	0.061	30/12/2021 15:38	17/02/2022 07:53	07/04/2022 00:07
49.6911 \pm 0.0001	0.059	01/01/2022 16:18	20/02/2022 08:54	11/04/2022 01:29
50.7484 \pm 0.0001	0.057	03/01/2022 19:03	23/02/2022 13:01	15/04/2022 06:59
51.8516 \pm 0.0001	0.055	06/01/2022 00:01	26/02/2022 20:27	19/04/2022 16:53
53.0039 \pm 0.0001	0.053	08/01/2022 07:19	02/03/2022 07:25	24/04/2022 07:30
54.2085 \pm 0.0001	0.051	10/01/2022 17:08	05/03/2022 22:09	29/04/2022 03:09
55.4692 \pm 0.0001	0.049	13/01/2022 05:39	09/03/2022 16:55	—
56.7899 \pm 0.0001	0.047	15/01/2022 21:03	13/03/2022 16:00	—
58.1750 \pm 0.0001	0.045	18/01/2022 15:32	17/03/2022 19:44	—
59.6294 \pm 0.0001	0.042	21/01/2022 13:21	22/03/2022 04:27	—
61.1583 \pm 0.0001	0.039	24/01/2022 14:44	26/03/2022 18:32	—
62.7678 \pm 0.0001	0.037	27/01/2022 19:59	31/03/2022 14:25	—

NOTE—Transit dates were calculated using the Transit Service Query Form on the NASA Exoplanet Archive (Akeson et al. 2013). We queried observable transits between December 3, 2021 through April 30, 2022. Dates presented in DD/MM/YYYY format. A machine-readable version of this table can be found here.

Foreman-Mackey, D., Luger, R., Agol, E., et al. 2021a, exoplanet: Gradient-based probabilistic inference for exoplanet data & other astronomical time series, v0.5.1, Zenodo, doi: [10.5281/zenodo.1998447](https://doi.org/10.5281/zenodo.1998447)

—. 2021b, The Journal of Open Source Software, 6, 3285, doi: [10.21105/joss.03285](https://doi.org/10.21105/joss.03285)

Frink, S., Röser, S., Neuhäuser, R., & Sterzik, M. F. 1997, A&A, 325, 613. <https://arxiv.org/abs/astro-ph/9704281>

Gaidos, E., Hirano, T., Beichman, C., et al. 2021, arXiv e-prints, arXiv:2110.10689. <https://arxiv.org/abs/2110.10689>

Gao, P., & Zhang, X. 2020, ApJ, 890, 93, doi: [10.3847/1538-4357/ab6a9b](https://doi.org/10.3847/1538-4357/ab6a9b)

Geweke, J. 1992, Bayesian Statistics IV. Oxford: Clarendon Press, ed. J. M. Bernardo, 169

Ginsburg, A., Sipőcz, B. M., Brasseur, C. E., et al. 2019, AJ, 157, 98, doi: [10.3847/1538-3881/aafc33](https://doi.org/10.3847/1538-3881/aafc33)

Ginzburg, S., Schlichting, H. E., & Sari, R. 2018, MNRAS, 476, 759, doi: [10.1093/mnras/sty290](https://doi.org/10.1093/mnras/sty290)

Grankin, K. N. 1999, Astronomy Letters, 25, 526

Gu, P.-G., Bodenheimer, P. H., & Lin, D. N. C. 2004, ApJ, 608, 1076, doi: [10.1086/420867](https://doi.org/10.1086/420867)

Gully-Santiago, M. A., Herczeg, G. J., Czekala, I., et al. 2017, ApJ, 836, 200, doi: [10.3847/1538-4357/836/2/200](https://doi.org/10.3847/1538-4357/836/2/200)

Hedges, C., Hughes, A., Zhou, G., et al. 2021, AJ, 162, 54, doi: [10.3847/1538-3881/ac06cd](https://doi.org/10.3847/1538-3881/ac06cd)

Howell, S. B., Sobeck, C., Haas, M., et al. 2014, PASP, 126, 398, doi: [10.1086/676406](https://doi.org/10.1086/676406)

Hunter, J. D. 2007, Computing in Science & Engineering, 9, 90, doi: [10.1109/MCSE.2007.55](https://doi.org/10.1109/MCSE.2007.55)

Jenkins, J. M., Twicken, J. D., McCauliff, S., et al. 2016, in Proc. SPIE, Vol. 9913, Software and Cyberinfrastructure for Astronomy IV, 99133E, doi: [10.1117/12.2233418](https://doi.org/10.1117/12.2233418)

Jin, S., Mordasini, C., Parmentier, V., et al. 2014, ApJ, 795, 65, doi: [10.1088/0004-637X/795/1/65](https://doi.org/10.1088/0004-637X/795/1/65)

Johnson, M. C., David, T. J., Petigura, E. A., et al. 2021, arXiv e-prints, arXiv:2110.10707. <https://arxiv.org/abs/2110.10707>

Kipping, D. M. 2013, MNRAS, 435, 2152, doi: [10.1093/mnras/stt1435](https://doi.org/10.1093/mnras/stt1435)

Kreidberg, L. 2015, PASP, 127, 1161, doi: [10.1086/683602](https://doi.org/10.1086/683602)

Krolikowski, D. M., Kraus, A. L., & Rizzuto, A. C. 2021, AJ, 162, 110, doi: [10.3847/1538-3881/ac0632](https://doi.org/10.3847/1538-3881/ac0632)

Lightkurve Collaboration, Cardoso, J. V. d. M., Hedges, C., et al. 2018, Lightkurve: Kepler and TESS time series analysis in Python, Astrophysics Source Code Library. <http://ascl.net/1812.013>

Lopez, E. D., & Fortney, J. J. 2013, ApJ, 776, 2, doi: [10.1088/0004-637X/776/1/2](https://doi.org/10.1088/0004-637X/776/1/2)

Luger, R., Agol, E., Foreman-Mackey, D., et al. 2019, AJ, 157, 64, doi: [10.3847/1538-3881/aae8e5](https://doi.org/10.3847/1538-3881/aae8e5)

- Luger, R., Bedell, M., Foreman-Mackey, D., et al. 2021, arXiv e-prints, arXiv:2110.06271.
<https://arxiv.org/abs/2110.06271>
- Luger, R., Kruse, E., Foreman-Mackey, D., Agol, E., & Saunders, N. 2018, *AJ*, 156, 99,
doi: [10.3847/1538-3881/aad230](https://doi.org/10.3847/1538-3881/aad230)
- Luhman, K. L. 2018, *AJ*, 156, 271,
doi: [10.3847/1538-3881/aae831](https://doi.org/10.3847/1538-3881/aae831)
- Nardiello, D., Piotto, G., Deleuil, M., et al. 2020, *MNRAS*, 495, 4924, doi: [10.1093/mnras/staa1465](https://doi.org/10.1093/mnras/staa1465)
- Newton, E. R., Mann, A. W., Tofflemire, B. M., et al. 2019, *ApJL*, 880, L17, doi: [10.3847/2041-8213/ab2988](https://doi.org/10.3847/2041-8213/ab2988)
- Oh, S., Price-Whelan, A. M., Hogg, D. W., Morton, T. D., & Spergel, D. N. 2017, *AJ*, 153, 257,
doi: [10.3847/1538-3881/aa6ffd](https://doi.org/10.3847/1538-3881/aa6ffd)
- Owen, J. E. 2020, *MNRAS*, 498, 5030,
doi: [10.1093/mnras/staa2784](https://doi.org/10.1093/mnras/staa2784)
- Owen, J. E., & Wu, Y. 2013, *ApJ*, 775, 105,
doi: [10.1088/0004-637X/775/2/105](https://doi.org/10.1088/0004-637X/775/2/105)
- Plavchan, P., Barclay, T., Gagné, J., et al. 2020, *Nature*, 582, 497, doi: [10.1038/s41586-020-2400-z](https://doi.org/10.1038/s41586-020-2400-z)
- Poppenhaeger, K., Ketzer, L., & Mallonn, M. 2021, *MNRAS*, 500, 4560, doi: [10.1093/mnras/staa1462](https://doi.org/10.1093/mnras/staa1462)
- Price-Whelan, A. M., Sipőcz, B. M., Günther, H. M., et al. 2018, *AJ*, 156, 123, doi: [10.3847/1538-3881/aabc4f](https://doi.org/10.3847/1538-3881/aabc4f)
- Ricker, G. R., Winn, J. N., Vanderspek, R., et al. 2015, *Journal of Astronomical Telescopes, Instruments, and Systems*, 1, 014003, doi: [10.1117/1.JATIS.1.1.014003](https://doi.org/10.1117/1.JATIS.1.1.014003)
- Salvatier, J., Wiecki, T. V., & Fonnesbeck, C. 2016, *PyMC3: Python probabilistic programming framework*.
<http://ascl.net/1610.016>
- Schlawin, E., Ilyin, I., Feinstein, A. D., et al. 2021, *Research Notes of the American Astronomical Society*, 5, 195, doi: [10.3847/2515-5172/ac1f2f](https://doi.org/10.3847/2515-5172/ac1f2f)
- Stassun, K. G., Oelkers, R. J., Pepper, J., et al. 2018, *AJ*, 156, 102, doi: [10.3847/1538-3881/aad050](https://doi.org/10.3847/1538-3881/aad050)
- Suárez Mascareño, A., Damasso, M., Lodieu, N., et al. 2021, arXiv e-prints, arXiv:2111.09193.
<https://arxiv.org/abs/2111.09193>
- The Theano Development Team, Al-Rfou, R., Alain, G., et al. 2016, arXiv e-prints, arXiv:1605.02688.
<https://arxiv.org/abs/1605.02688>
- Van Der Walt, S., Colbert, S. C., & Varoquaux, G. 2011, *Computing in Science & Engineering*, 13, 22
- Vissapragada, S., Stefánsson, G., Greklek-McKeon, M., et al. 2021, arXiv e-prints, arXiv:2108.05358.
<https://arxiv.org/abs/2108.05358>
- Wang, L., & Dai, F. 2019, *ApJL*, 873, L1,
doi: [10.3847/2041-8213/ab0653](https://doi.org/10.3847/2041-8213/ab0653)
- Wichmann, R., Krautter, J., Schmitt, J. H. M. M., et al. 1996, *A&A*, 312, 439
- Wichmann, R., Torres, G., Melo, C. H. F., et al. 2000, *A&A*, 359, 181
- Zhou, G., Quinn, S. N., Irwin, J., et al. 2021, *AJ*, 161, 2,
doi: [10.3847/1538-3881/abba22](https://doi.org/10.3847/1538-3881/abba22)